ASME Journal of Engineering and Science in Medical Diagnostics and Therapy
Online journal at:
https://asmedigitalcollection.asme.org/medicaldiagnostics

Harmonics of Pulsatile Pressure at Different Ages and Its Effect on Other Pulsatile Parameters and Waveform-Based Clinical Indices

Zhili Hao
Department of Mechanical and Aerospace Engineering,
Old Dominion University,
Norfolk, VA 23529
e-mail: zlhao@odu.edu

Pulsatile pressure at an artery is a collection of harmonics of the heartbeat. This study examines harmonics of pulsatile pressure at different ages and its effect on other pulsatile parameters and waveform-based clinical indices. Based on a vibrating-string model of the arterial tree, wave velocity and characteristic impedance are related to arterial stiffness and radius. Blood velocity, wall shear stress (WSS), and driving force on the left ventricle (LV) are related to pulsatile pressure. Reflection magnitude and return time are related to input impedance. These relations are applied to pulsatile pressure and blood velocity at the ascending aorta (AA) and the carotid artery (CA) at different ages in a database to calculate harmonics of all the pulsatile parameters and reflection magnitude and return time at each harmonic. Harmonics of pulsatile pressure varies with aging and between the two arteries. Reflection magnitude and return time vary between harmonics. While wave reflection manifests the arterial tree (i.e., arterial stiffness and radius) and termination, harmonics of pulsatile pressure is a combination of the LV, the arterial tree, and termination. Harmonics of pulsatile pressure dictates harmonics of WSS and affects endothelial function. Harmonics of pulsatile pressure needs to serve as an independent clinical index indicative of the LV function and endothelial function. Reflection magnitude and return time of the 1st harmonic of pulsatile pressure serve as clinical indices indicative of arterial stiffness and radius.
[DOI: 10.1115/1.4062570]

Keywords: pulsatile parameter waveform, harmonics-dependence, wave reflection, input impedance, reflection magnitude, return time

1 Introduction

As compared with their amplitudes, waveforms of pulsatile parameters at an artery carry more physiological and pathological information of the cardiovascular (CV) condition [1–15]. Various clinical indices based on pulsatile parameter waveform have been defined for assessment of the CV condition. For instance, blood flow pulsatility index (FPI) and time-averaged wall shear stress (TAWSS) over pulse cycle at the carotid artery (CA) are based on blood velocity waveform [9–12] and wall shear stress (WSS) waveform [13–15], respectively. Although pulsatile parameters at the CA are more accessible, pulsatile parameters at the ascending aorta (AA) are more relevant to the left ventricle (LV) function, due to its direct connect to the LV [1–8]. Waveforms of pulsatile pressure and blood velocity at the AA have been analyzed for input impedance (ratio of pulsatile pressure to blood velocity with wave reflection) [2,16–18]. Pulsatile pressure waveform at the AA has been analyzed for return time (time difference between the forward waveform and the reflected waveform), reflection magnitude (amplitude ratio of the forward waveform to the reflected waveform), as well as augmentation index (AI, the ratio of augmented pressure to pulsatile pressure) [1,2]. As compared with arterial stiffness (commonly measured as pulse wave velocity (PWV)), these clinical indices have shown their independent values, although they are all considered to be indicative of arterial stiffness [1–3,18].

All the waveform-based clinical indices are aimed to capture mechanical changes at an artery between healthy condition and an unhealthy condition, since pulsatile parameter waveform is found to be affected by arterial mechanical changes, with the latter implying pathological changes. A pulsatile parameter at an artery comprises of the forward waves and reflected waves. Thus, pulsatile parameter waveform is affected by wave reflection. It has been well recognized that arterial stiffness plays a role in wave reflection [1–18]. Since waveform-based clinical indices carry their independent values, it might be inferred that pulsatile parameter waveform is associated with other factors, besides arterial stiffness. In a recent numerical study, both arterial stiffness and radius were found to affect wave reflection [1]. Meanwhile, a clinical study [3] identified pulsatile pressure amplitude and arterial radius as two contributors to carotid FPI and further pointed out the existence of other factors underlying carotid FPI. Since pulsatile pressure amplitude is related to wave

Contributed by the Applied Mechanics Division Technical Committee on Dynamics & Control of Structures & Systems (AMD-DCSS) of ASME for publication in the Journal of Engineering and Science in Medical Diagnostics and Therapy. Manuscript received February 28, 2023; final manuscript received May 10, 2023; published online June 14, 2023. Assoc. Editor: Shijia Zhao.

reflection, it might be inferred that besides arterial stiffness and radius, there are other factors underlying carotid FPI.

Other than wave reflection, a pulsatile parameter is a collection of harmonics of the heartbeat [1,16]. Thus, pulsatile parameter waveform is also affected by harmonics of a pulsatile parameter. It has been found that the input impedance at the AA varies with harmonics and carries clinical values [1,16]. Harmonics-dependence of input impedance translates to harmonics-dependence of wave reflection [16] and thus return time [19]. Yet, the studies on return time at the AA have neglected such dependence, which explains the difficulty in identifying the foot of the reflected waveform from pulsatile pressure waveform for calculating return time [1,2]. Moreover, the majority of the studies on the CV system has neglected harmonics of a pulsatile parameter, except that FPI and TAWSS at the CA and reflection magnitude and AI at the AA manifest harmonics of a pulsatile parameter to a very limited extent [19]. To date, there are only a moderate number of studies on harmonics of a pulsatile parameter [20–25]. These studies on harmonics of a pulsatile parameter have mostly focused on pulsatile pressure at the radial artery (RA), and have correlated changes in harmonics of pulsatile pressure to different conditions, such as diabetes [20], aging [21], coronary artery disease [22,23], and Alzheimer's disease [24]. Additionally, the influence of different daily activities on harmonics of pulsatile pressure at the RA was also studied [25]. Given the influence of daily activities on arterial stiffness and radius, it might be inferred that harmonics of a pulsatile parameter is affected by arterial stiffness and radius, similar to wave reflection.

Endothelial cells (EC) lining the inner surface of the arterial wall are continuously exposed to WSS. EC transduce WSS into biochemical signals that regulate gene expression and cell behavior [26,27]. Thus, WSS is recognized as an essential mechanical cue for vascular growth, remodeling, and homeostasis [26,27]. EC have evolved sophisticated mechanosensing abilities to detect distinct features of WSS and regulate vascular homeostasis and remodeling accordingly [13,26,27]. These features include both the amplitude and harmonics of WSS (or WSS waveform). Changes in WSS amplitude and waveform are thought to undermine regulation behavior of EC and ultimately lead to endothelial dysfunction, which initiates the development of atherosclerosis. Besides WSS, EC are continuously exposed to circumferential strain (CS) in the arterial wall. Endothelial function is found to be synergistically regulated by WSS and CS [28]. While harmonics of CS and harmonics of pulsatile pressure are identical, harmonics of WSS greatly differs from harmonics of pulsatile pressure [14,19]. To date, higher harmonics of WSS are known to contribute to a larger WSS amplitude [8]. Yet, to the author's best knowledge, how harmonics of pulsatile pressure affects harmonics of WSS has seldom been studied, due to mathematical difficulty in calculating WSS waveform [14], and consequently the effect of harmonics of pulsatile pressure on relation of WSS versus CS remains unknown.

Recently, the author developed a vibrating-string model of the arterial tree [19], which shows that wave velocity and characteristic impedance at an artery are both harmonics-dependent and impedance at termination of the arterial tree is also harmonics-dependent and must be included in wave reflection. This vibrating-string model provides a theoretical basis for harmonics-dependence of wave reflection at the AA and a theoretical proof on the role of arterial stiffness and radius in wave reflection. By applying this vibrating-string model to pulsatile pressure and blood velocity at the AA and the CA at different ages in a database [29], this study aims to examine harmonics of pulsatile pressure at different ages and its effect on other pulsatile parameters and waveform-based clinical indices, and thus gain a better understanding of physical implications and affecting factors of harmonics of pulsatile pressure and waveform-based clinical indices.

The rest of the paper is organized as follows. Section 2 presents the vibrating-string model and provides theoretical expressions of wave velocity and characteristic impedance in terms of arterial stiffness and radius, and theoretical expressions of blood velocity, WSS, and radial displacement of the arterial wall in terms of pulsatile pressure. Theoretical expressions of the input power at the AA and driving force on the LV are derived. Theoretical expressions of reflection magnitude and return time in terms of input impedance are also provided. The data-processing algorithms for analyzing pulsatile pressure and blood velocity at different ages are presented. In Sec. 3, the calculated results at different ages are described. The effect of aging on harmonics and waveform of the pulsatile parameters and the *1st* harmonic of pulsatile pressure is examined. Section 4 focuses on clarifying the cause of harmonics-dependence of wave transmission and wave reflection, and exploring possible affecting factors of wave transmission, wave reflection, and harmonics of pulsatile pressure. Inconsistency of some definitions in clinical studies with their physical implications is identified, and physical implications of waveform-based clinical indices are clarified. The difference in harmonics of pulsatile pressure at different ages and between the two arteries is discussed for its physiological implications and potential clinical applications. In Sec. 5, the key findings from this study are summarized.

2 Methods

2.1 A Vibrating-String Model of the Arterial Tree. The details about the vibrating-string model of the arterial tree can be found in the literature [19]. For completeness, a brief description of the vibrating-string model and theoretical expressions related to this study are presented here.

2.1.1 Standard One-Dimensional Wave Equation for Arterial Pulse Wave Propagation. Pulsatile pressure $\Delta p(x,t)$ at position x along the arterial tree is a collection of harmonics of the heartbeat

$$\Delta p(x,t) = \sum_n (A_n e^{-ik_n x} + B_n e^{ik_n x}) e^{in\omega t} \tag{1a}$$

where A_n and B_n denote the forward and reflected pressure wave amplitudes of the nth harmonic, respectively, with ω as the fundamental angular frequency of the heartbeat; and $k_n = n\omega/c_n$ is the nth wave number, with c_n being the nth wave velocity. Pulsatile pressure causes radial displacement $\eta(x,t)$ of the arterial wall and blood velocity $u(x,t)$ (averaged across the lumen) in blood flow, which further causes wall shear stress (WSS) $\tau_w(x,t)$ [19]

$$\eta(x,t) = \frac{a^2}{Eh} \sum_n \left(A_n e^{-ik_n x} + B_n e^{ik_n x}\right) e^{in\omega t} \tag{1b}$$

$$u(x,t) = \frac{1}{\rho_b} \sum_n \frac{1 - F_{10}}{c_n} \left(A_n e^{-ik_n x} - B_n e^{ik_n x}\right) e^{in\omega t} \tag{1c}$$

$$\tau_w(x,t) = -\frac{a}{2} \sum_n \frac{in\omega F_{10}}{c_n} \left(A_n e^{-ik_n x} - B_n e^{ik_n x}\right) e^{in\omega t} \tag{1d}$$

where E, a, and h denote the circumferential elasticity, inner radius, and thickness of the arterial wall, respectively, and ρ_b is blood density. While wave reflection augments pulsatile pressure and radial wall displacement, it reduces blood velocity and WSS.

In Eqs. (1*c*) and (1*d*), F_{10} results from fluid-loading on the arterial wall:

$$F_{10} = \frac{2J_1(\alpha_0)}{\alpha_0 J_0(\alpha_0)} \text{ (harmonics} - \text{dependent, complex)} \tag{2}$$

where $\alpha_0^2 = i^3\alpha^2$ with $\alpha = a\sqrt{\rho_b n\omega/\mu}$ being the Womersley number and μ being blood viscosity. Due to harmonics-dependence of the Womersley number, F_{10} is harmonics-dependent and takes complex values. Given that inertial term of the arterial wall is negligible relative to its elastic term, pulsatile pressure is related to radial wall displacement by

$$\eta(x,t) = \frac{a^2}{Eh}\Delta p(x,t) \tag{3}$$

Thus, pulsatile pressure waveform and radial wall displacement waveform are identical. The wave velocity for the nth harmonic is given by Hao [19]

$$c_n = c_0\sqrt{(1-F_{10})} \text{ with } c_0 = \text{PWV} = \sqrt{\frac{Eh}{2\rho_b a}} \tag{4}$$

Note that c_0 is the same as PWV (referred to as arterial stiffness) in clinical studies and is independent of harmonics.

Based on Eq. (1), the standard one-dimensional (1D) wave equations for radial wall displacement and blood velocity can be written as

$$\frac{\partial^2\eta}{\partial t^2} = c^2\frac{\partial^2\eta}{\partial x^2} \text{ and } \frac{\partial^2 u}{\partial t^2} = c^2\frac{\partial^2 u}{\partial x^2} \tag{5}$$

The standard 1D wave equation for the transverse displacement $y(x,t)$ of a vibrating string is given by Feaver [27] and Zhao [28]

$$\rho_L\frac{\partial^2 y}{\partial t^2} = T\frac{\partial^2 y}{\partial x^2} \tag{6}$$

where ρ_L and T denote linear density and tension of the vibrating string, respectively. Comparison of Eq. (5) with Eq. (6) leads to a vibrating-string model of an artery with the following equivalent linear density and equivalent tension:

$$\rho_L = \rho_b\pi a^2 \text{ and } T = \frac{\pi Eh}{2}a(1-F_{10}) \tag{7}$$

Note that $1-F_{10}$ is harmonics-dependent at small arteries, such as the carotid artery (CA) and the radial artery (RA), and $1-F_{10} \cong 1$ is harmonic-independent at the AA, due to its large size.

2.1.2 Characteristic Impedance, Input Impedance, Reflection Magnitude, and Return Time. As shown in Fig. 1, the arterial tree can be treated as a uniform vibrating string. Being more aligned with transverse displacement of a vibrating string, radial wall displacement is chosen for defining the terms related to wave transmission and wave reflection. The arterial tree starts with the AA at $x=0$ and ends at termination $x=L_T$. Radial wall displacement at position x for the nth harmonic is written as

$$\eta_n(x,t) = (A_n e^{-ik_n x}e^{-\gamma_n x} + B_n e^{ik_n x}e^{\gamma_n x})e^{in\omega t} \tag{8}$$

where A_n and B_n denote forward and backward wave amplitudes, respectively, of the nth harmonic at the AA. Wave transmission is quantified by wave number k_n and transmission loss γ_n:

$$k_n = \frac{n\omega}{\text{Re}(c_n)} \text{ and } \gamma_n = \frac{n\omega}{\text{Im}(c_n)} \tag{9}$$

where $\text{Re}(c_n)$ and $\text{Im}(c_n)$ denote the real part and the imaginary part of c_n, respectively.

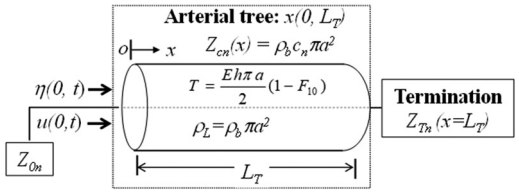

Fig. 1 Schematics of a uniform vibrating-string model for arterial pulsatile wave propagation

The nth driving force $F_n(x,t)$ becomes

$$F_n(x,t) = -T\partial\eta_n/\partial x = \rho_L c_n in\omega(A_n e^{-ik_n x}e^{-\gamma_n x} - B_n e^{ik_n x}e^{\gamma_n x})e^{in\omega t} \tag{10}$$

The nth mechanical impedance $Z_n(x)$ is defined as [30]

$$Z_n(x) = \frac{F_n}{\partial\eta_n/\partial t} = \rho_L c_n\frac{(A_n e^{-ik_n x}e^{-\gamma_n x} - B_n e^{ik_n x}e^{\gamma_n x})}{(A_n e^{-ik_n x}e^{-\gamma_n x} + B_n e^{ik_n x}e^{\gamma_n x})} \tag{11}$$

Accordingly, the nth characteristic impedance $Z_{cn}(x)$ at an artery becomes

$$Z_{cn}(x) = \sqrt{\rho_L T} = \rho_b c_0\pi a^2\sqrt{(1-F_{10})} \tag{12}$$

The nth input impedance Z_{0n} at $x=0$ is given by

$$Z_{0n} = Z_{cn}\frac{A_n - B_n}{A_n + B_n} = Z_{cn}G_n^{-1}e^{-i\phi_n} \text{ with } \frac{A_n - B_n}{A_n + B_n} = G_n^{-1}e^{-i\phi_n} \tag{13}$$

Wave reflection is quantified by reflection coefficient. Based on Eq. (13), the nth reflection efficient R_n at $x=0$ is written as

$$R_n = r_n e^{i\psi_n} = \frac{B_n}{A_n} = \frac{G_n e^{i\phi_n} - 1}{G_n e^{i\phi_n} + 1} = \frac{{G_n}^2 - 1 + 2G_n\sin\phi_n i}{{G_n}^2 + 2G_n\cos\phi_n + 1} \tag{14}$$

As the phase delay of the reflected nth harmonic relative to the forward nth harmonic, ψ_n takes negative values. Accordingly, the nth reflection magnitude r_n and return time Δt_n become

$$r_n = \left|\frac{G_n e^{i\phi_n} - 1}{G_n e^{i\phi_n} + 1}\right| \text{ and } \Delta t_n = \frac{-\psi_n}{n\omega} = \frac{-a\tan\frac{2G_n\sin\phi_n}{{G_n}^2-1}}{n\omega} \tag{15}$$

2.1.3 Input Power at the Ascending Aorta and Driving Force on the Left Ventricle. Other than radial wall displacement, pulsatile pressure also causes blood velocity. Based on Eq. (5), the above analysis applies to blood velocity. In this vibrating-string model, blood velocity needs to be treated as transverse displacement with unit m, instead of m/s, and wave reflection augments blood velocity. Then, the nth radial wall displacement is related to the nth blood velocity by

$$u_n(x,t) = \frac{2c_n}{a}\eta_n(x,t) \tag{16}$$

Based on Eqs. (10) and (11), the nth input power at the AA associated with radial wall displacement and blood velocity are written as [30,31]

$$P_{n-\eta} = \frac{1}{2}\left(\frac{\partial\eta_n}{\partial t}\right)^2 Z_{0n} = \frac{1}{2}(n\omega\eta_n)^2 Z_{0n} \tag{17a}$$

$$P_{n-u} = \frac{1}{2}\left(\frac{\partial u_n}{\partial t}\right)^2 Z_{0n} == \frac{1}{2}(n\omega u_n)^2 Z_{0n} = \frac{4c_n^2}{a^2}P_{n-\eta} \tag{17b}$$

Since $c_n/a \gg 1$, the input power associated with radial wall displacement can be neglected, as compared with that associated with blood velocity. For comparison, the nth input power measured in clinical studies is defined as [18]

$$P_{n-\text{meas}} = \frac{\pi a^2}{2}\Delta p_n u_n = \frac{1}{(n\omega)^2}P_{n-u} \tag{18}$$

As shown in Fig. 2(*a*), driving force on the LV excites pulsatile waves, which propagate along the arterial tree and reflect back at termination. Since being connected to the LV, the arterial tree interferes with the response of the LV to driving force. Given its

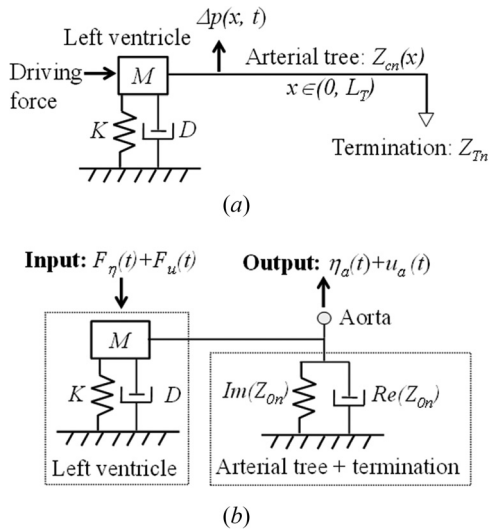

Fig. 2 Schematics of (*a*) the whole system for arterial pulsatile wave propagation: the LV, the arterial tree, and termination, and (*b*) a lumped-element model for the LV-artery interaction (Note: $M = 0.3$ kg, $K = M{\cdot}\omega^2$, and $D = \sqrt{KM}/Q$ with $Q = 100$ are used for calculation of the driving force on the LV at all ages, due to a lack of ECG data)

time-harmonic motion, the LV is treated as a mechanical oscillator with mass M, string stiffness K, and damping coefficient D. The driving force sees the arterial tree and termination as the input impedance. The real and the imaginary parts of the input impedance represent energy transmitted and energy reflected at the AA, respectively, and thus function as a damper and a spring, respectively, as shown in Fig. 2(*b*). Then, the driving force on the LV is related to radial wall displacement and blood velocity at the AA by Hao [19] and Kinsler [30]

$$F_\eta(t) = \sum_n in\omega\left\{D + i\left(Mn\omega - \frac{K}{n\omega}\right) + \mathrm{Re}(Z_{0n}) + i\,\mathrm{Im}(Z_{0n})\right\}\eta_a(t) \tag{19a}$$

$$F_u(t) = \sum_n in\omega\left\{D + i\left(Mn\omega - \frac{K}{n\omega}\right) + \mathrm{Re}(Z_{0n}) + i\,\mathrm{Im}(Z_{0n})\right\}\frac{2c_n}{a}\eta_a(t) \tag{19b}$$

where $\eta_a(t)$ is radial wall displacement at the AA, and $\mathrm{Re}(Z_{0n})$ and $\mathrm{Im}(Z_{0n})$ denote the real and imaginary parts of the input impedance, respectively. The driving force for blood velocity at the AA is well above that for radial wall displacement. The input impedance in Eq. (19) is related to measured input impedance $Z_{0n\text{-meas}}$ in clinical studies by

$$Z_{0n} = \frac{\left[(\rho_b c_0)^2 \pi a^2\right]_{\mathrm{AA}}}{Z_{0n-\mathrm{meas}}} \tag{20}$$

2.2 Data-Processing Algorithms. In this study, simulated pulsatile pressure waveforms and blood velocity waveforms in time domain at the AA and the CA of healthy virtual subjects at different ages (25 yr–75yr) in a database [29] were chosen for analysis. These simulated waveforms were verified by comparing with corresponding in vivo data and well-reproduced age-related changes in hemodynamic parameters [26]. Arterial stiffness and radius (i.e., PWV and a) at different ages were provided in the database. Based on the database, $\rho_b = 1066\,\mathrm{kg/m^3}$ and $\mu = 0.0025$ Pa·s were used in the calculation. These simulated data were referred to as measured data here. All the calculation was conducted in MATLAB.

Fast Fourier transform (FFT) analysis was first conducted on pulsatile pressure waveform and blood velocity waveform in time domain to obtain the amplitudes and phases of their first ten harmonics [16]

$$\Delta p(t) = \sum_{n=1}^{10} \Delta p_n \cos(n\omega t + \alpha_n) \tag{21a}$$

$$u(t) = \sum_{n=1}^{10} u_n \cos(n\omega t + \beta_n) \tag{21b}$$

where Δp_n and α_n denote the amplitude and phase of the nth harmonic in pulsatile pressure, respectively; and u_n and β_n denote the amplitude and phase of the nth harmonic in blood velocity, respectively. The nth measured input impedance was then calculated [16]

$$Z_{0n-\mathrm{meas}}(x) = \frac{\Delta p_n(t)}{u_n(t)} = \frac{\Delta p_n}{u_n} e^{i(\alpha_n - \beta_n)} = Z_{cn-\mathrm{meas}} G_n e^{i\phi_n} \text{ with } Z_{cn-\mathrm{meas}} = \frac{\rho_b c_0}{\sqrt{1 - F_{10}}} \tag{22}$$

where $Z_{\mathrm{cn\text{-}meas}}$ is the characteristic impedance used in clinical studies. Based on the given arterial stiffness and radius, characteristic impedance was calculated, and consequently G_n and ϕ_n were obtained.

To calculate the forward and reflected waveforms, pulsatile pressure waveform and blood velocity waveform need to be combined for separating the forward waves from the reflected waves [16]

$$A_n e^{in\omega t} = \frac{\Delta p_n(t)}{2} + Z_{cn-\mathrm{meas}} \frac{u_n(t)}{2} \tag{23a}$$

$$B_n e^{in\omega t} = \frac{\Delta p_n(t)}{2} - Z_{cn-\mathrm{meas}} \frac{u_n(t)}{2} \tag{23b}$$

where A_n and B_n are the nth forward and reflected wave amplitudes, respectively. By substituting Eqs. (23) into (1*d*), WSS waveform was also calculated. FFT analysis on WSS was followed to obtain its first ten harmonics

$$\tau_w(t) = \sum_{n=1}^{10} \tau_{wn} \cos(n\omega t + \theta_n) \tag{24}$$

where τ_{wn} and θ_n denote the amplitude and phase of the nth harmonic in WSS, respectively.

By substituting the calculated values of G_n and ϕ_n into Eq. (15), reflection magnitude and return time for each harmonic in pulsatile pressure were obtained. Substituting the measured input impedance into Eq. (20) led to the input impedance defined in the vibrating-string model. Based on Eqs. (17) and (18), the input power at the AA defined in the vibrating-string model and in clinical studies were calculated. The driving force associated with blood velocity was also calculated based on Eq. (19*b*).

3 Results

3.1 Harmonics of Pulsatile Pressure, Blood Velocity, and Wall Shear Stress. Figures 3(*a*)–3(*d*) shows the pulsatile pressure waveforms and blood velocity waveforms at the AA and the CA reconstructed using their harmonics. Figures 3(*e*) and 3(*f*) show the calculated WSS waveforms. While pulsatile pressure amplitude increases with aging at both arteries, blood velocity amplitude and WSS amplitude decrease with aging at both arteries. Meanwhile, the

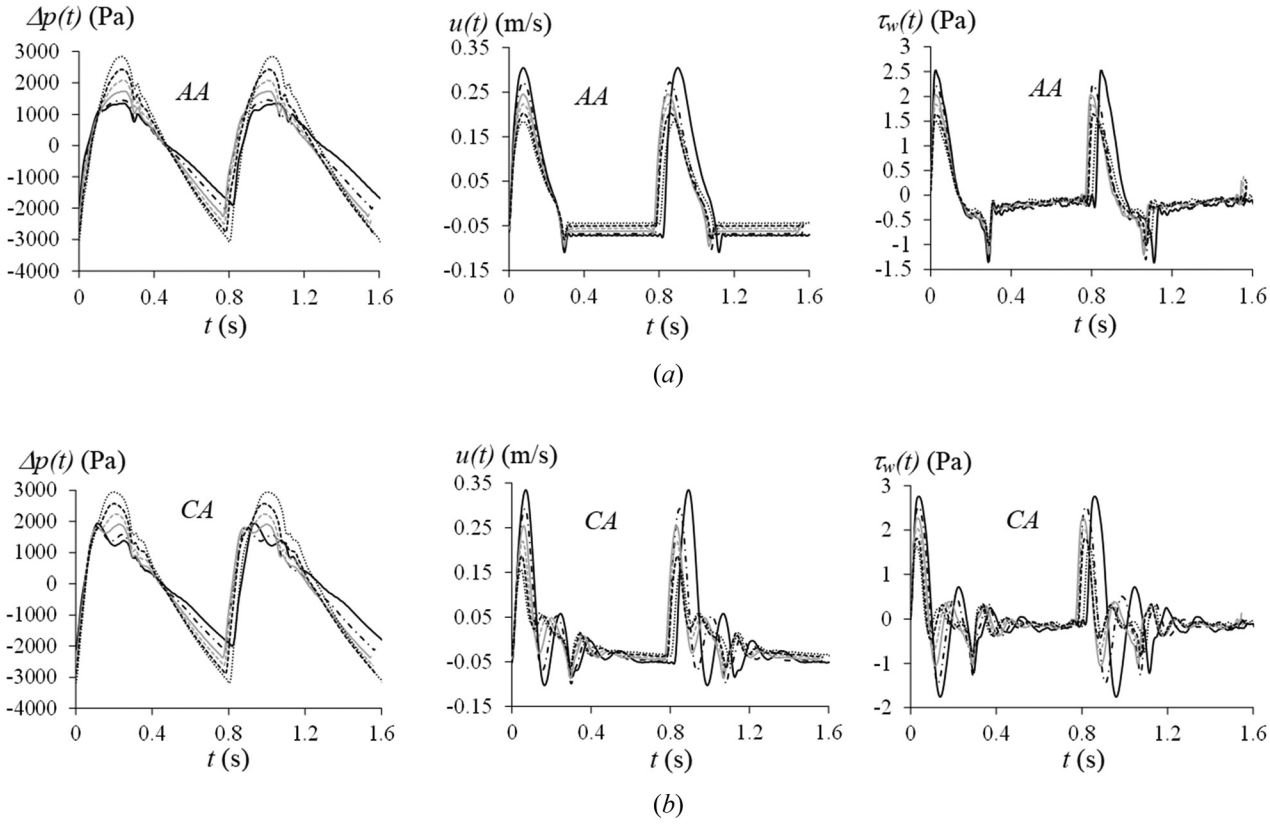

Fig. 3 Waveforms of pulsatile parameters at different ages: (*a*) pulsatile pressure (*b*) blood velocity (*c*) wall shear stress at the AA, and (*d*) pulsatile pressure (*e*) blood velocity (*f*) wall shear stress at the CA (25 yr: black solid, 35 yr: black dashdotted, 45 yr: gray solid, 55 yr: gray dashed, 65 yr: black dashed, 75 yr: black dotted)

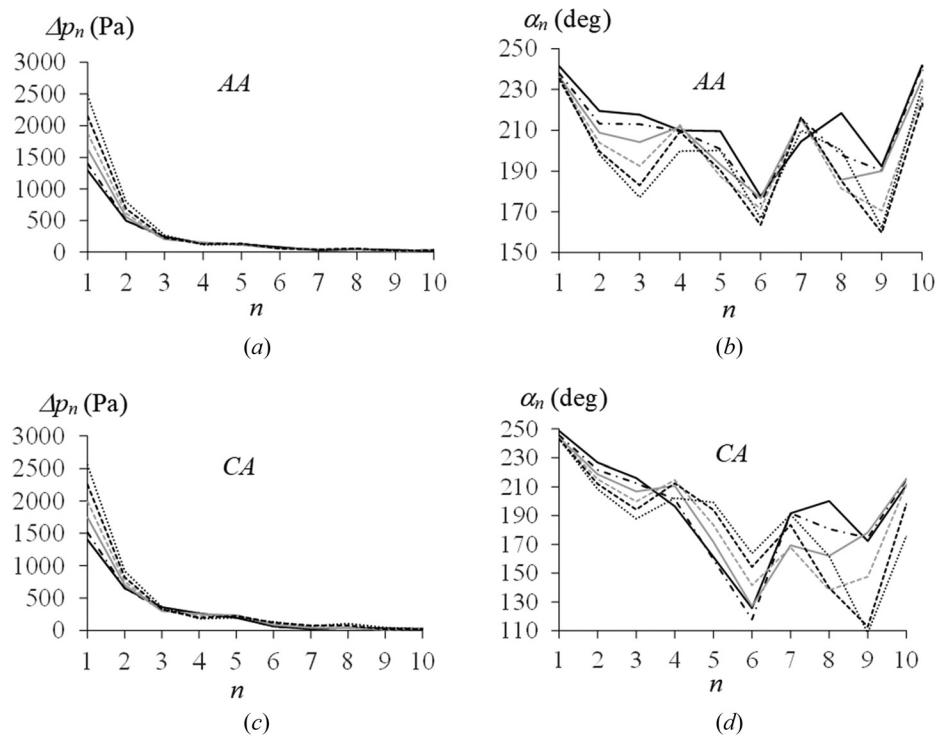

Fig. 4 The first ten harmonics of pulsatile pressure at different ages: (*a*) amplitude (*b*) phase at the AA, and (*c*) amplitude (*d*) phase at the CA (25 yr: black solid, 35 yr: black dashdotted, 45 yr: gray solid, 55 yr: gray dashed, 65 yr: black dashed, 75 yr: black dotted)

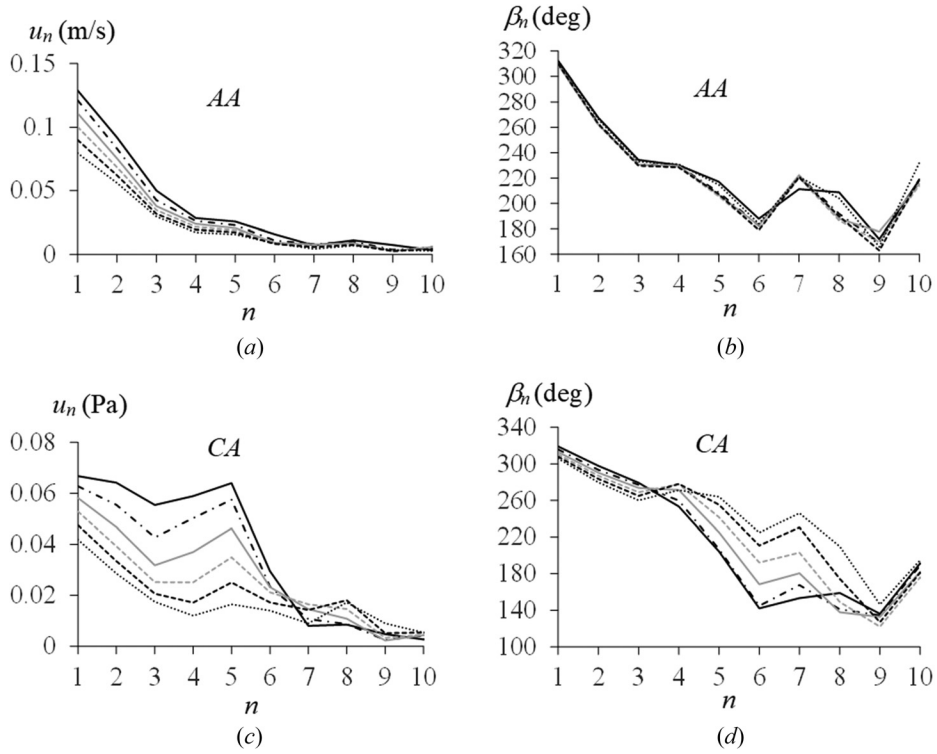

Fig. 5 The first ten harmonics of blood velocity at different ages: (*a*) amplitude (*b*) phase at the AA, and (*c*) amplitude (*d*) phase at the CA (25 yr: black solid, 35 yr: black dashdotted, 45 yr: gray solid, 55 yr: gray dashed, 65 yr: black dashed, 75 yr: black dotted)

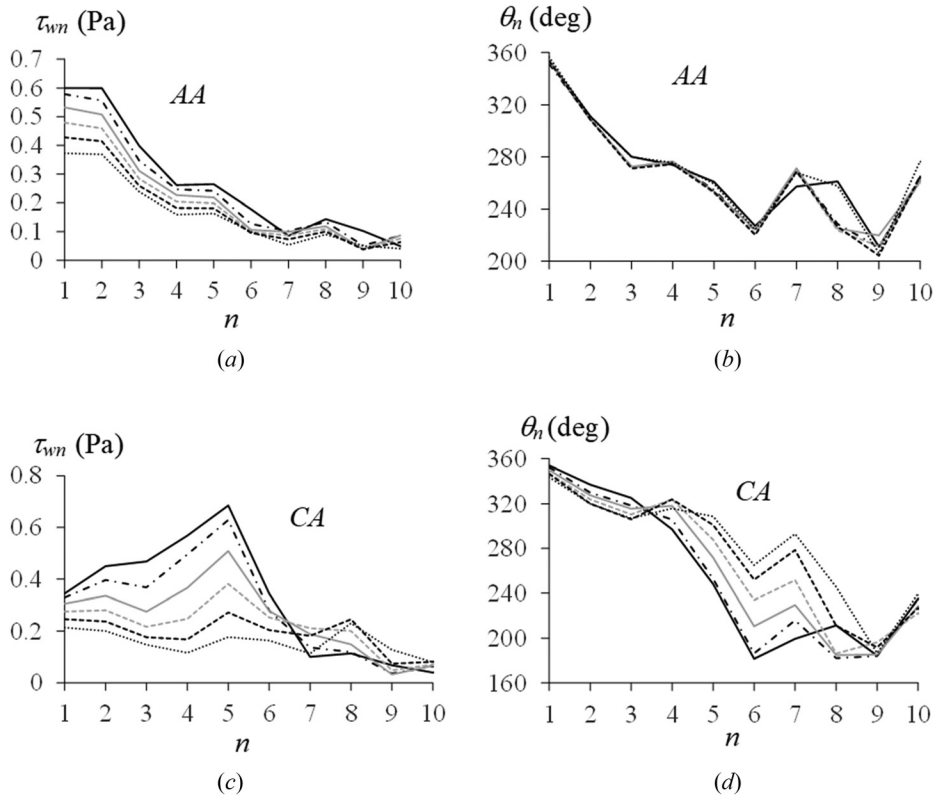

Fig. 6 The first ten harmonics of WSS at different ages: (*a*) amplitude (*b*) phase at the AA, and (*c*) amplitude (*d*) phase at the CA (25 yr: black solid, 35 yr: black dashdotted, 45 yr: gray solid, 55 yr: gray dashed, 65 yr: black dashed, 75 yr: black dotted)

waveforms of the three pulsatile parameters vary with both aging and between the two arteries.

As shown in Fig. 4, the amplitudes of the 1st and 2nd harmonics are dominant in pulsatile pressure, with the 1st harmonic being much more pronounced, and the amplitudes of the harmonics decrease with higher *n*-levels at the AA and the CA at all ages. The amplitudes of the 1st and 2nd harmonics show a definitive increasing trend with aging. The amplitudes of those higher harmonics do not show noticeable changes with aging. The phases of the *1*st and *2*nd harmonics show a definitive decreasing trend with aging, but the phases of those higher harmonics vary randomly between harmonics and do not show any changing trend with aging. Overall, it might be inferred that the 1st and 2nd harmonics in pulsatile pressure are less dominant but retain larger phases at young age, as compared with at old age.

As shown in Figs. 5(*a*) and 5(*b*), the amplitudes of harmonics of blood velocity decrease with higher *n*-levels at the AA. The 1st and 2nd harmonics in blood velocity are less dominant, as compared with their counterparts in pulsatile pressure. The amplitudes of harmonics of blood velocity all decrease with aging. Overall, the phases of harmonics of blood velocity show a decreasing trend with higher *n*-level, but do not vary noticeably with aging. As shown in Figs. 5(*c*) and 5(*d*), the 1st to 5th harmonics in blood velocity at the CA become dominant at all ages. The amplitudes of the 1st to 5th harmonics all decrease with aging. The phases of the 1st to 3rd harmonics all decrease with aging, but the phases of all the rest harmonics do not show a clear changing trend with aging. Overall, the phases of harmonics of blood velocity show a decreasing trend with higher *n*-level. The high pulsatility in blood velocity waveform at the CA in Fig. 2(*d*) might result from the higher harmonics, as compared with their counterparts at the AA.

As shown in Figs. 6(*a*) and 6(*b*), the amplitudes of 1st and 2nd harmonics of WSS at the AA are quite similar at all ages. The amplitudes of the rest harmonics decrease with higher *n*-levels. Overall, the phases of the harmonics of WSS show a decreasing trend with higher *n*-levels. While the amplitudes of all the harmonics decrease with aging, the phases of the harmonics do not show any noticeable change with aging. As shown in Figs. 6(*c*) and 6(*d*), the 5th harmonic of WSS at the CA has the largest amplitude among the ten harmonics. Although the 1st to 5th harmonics at the CA are dominant, the 6th to 10th harmonics are not negligible, as compared with their counterparts in pulsatile pressure and blood velocity. Overall, the phases of harmonics of WSS decrease with high *n*-levels at the CA. The amplitudes of the 1st to 5th harmonics and the phases of the 1st to 3rd harmonics show a decreasing trend with aging.

3.2 Wave Reflection: Reflection Magnitude and Return Time Versus Harmonics. Figures 7(*a*) and 7(*b*) show the amplitude and phase of the measured input impedance at the AA. The input impedance at the 1st and 2nd harmonics is dominant, as compared with that for the rest harmonics. The input impedance at the 1st and 2nd harmonics increases noticeably with aging. The phases of input impedance at lower harmonics are negative. The negative phase of the input impedance for the 1st harmonics increases with aging. As shown in Figs. 7(*c*) and 7(*d*), the input impedance for the 1st and 2nd harmonics at the CA are less dominant, as compared with their counterparts at the AA. Overall, the input impedance at the first six harmonics increases with aging. It seems like that the phase of the input impedance at the 2nd harmonics remains the same for all the ages. The negative phase of the input impedance for the 1st harmonics decreases with aging.

As shown in Figs. 8(*a*) and 8(*b*), reflection magnitude drops fast from the 1st harmonic to the 3rd harmonic and then remain unchanged at higher *n*-levels at the AA. The reflection magnitudes for the 1st to 3rd harmonics increase with aging, with reflection magnitude for the 3rd harmonic increasing fastest with aging. The return time shows a decreasing trend with high harmonics at all ages. The return time for the 1st harmonic is the longest and drops greatly with aging. The return time for the rest harmonics does not show a noticeable changing trend with aging. As shown in Figs. 8(*c*) and

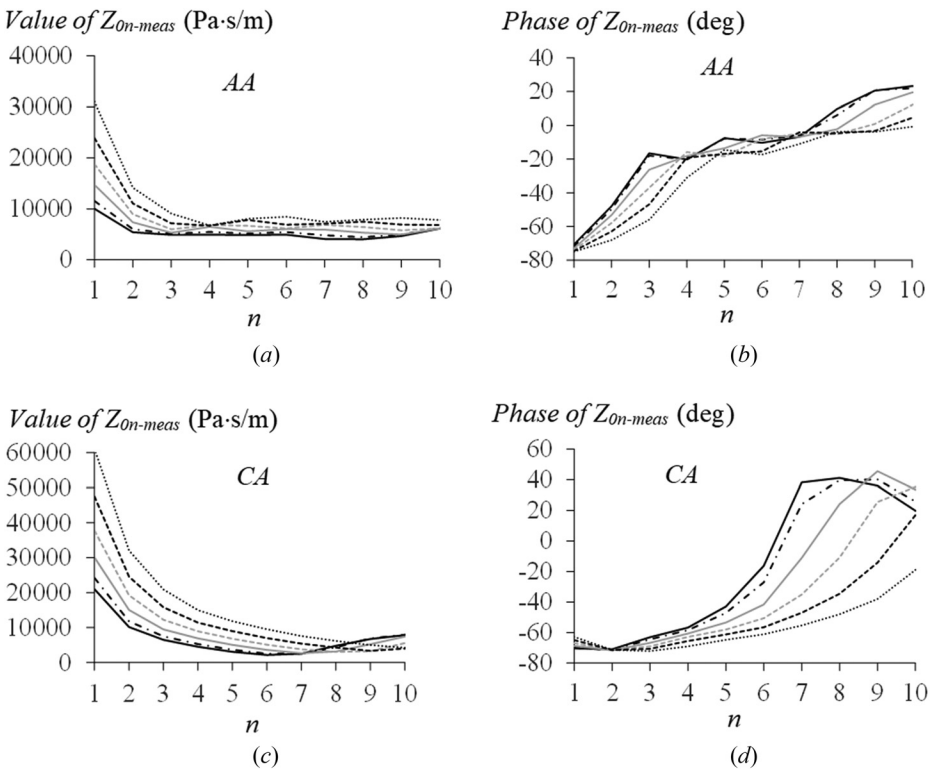

Fig. 7 Measured input impedance $Z_{0n\text{-meas}}$ defined as $\Delta p(t)/u(t)$ varies with harmonics at different ages: (*a*) amplitude (*b*) phase at the AA, and (*c*) amplitude (*d*) phase at the CA (25 yr: black solid, 35 yr: black dashdotted, 45 yr: gray solid, 55 yr: gray dashed, 65 yr: black dashed, 75 yr: black dotted)

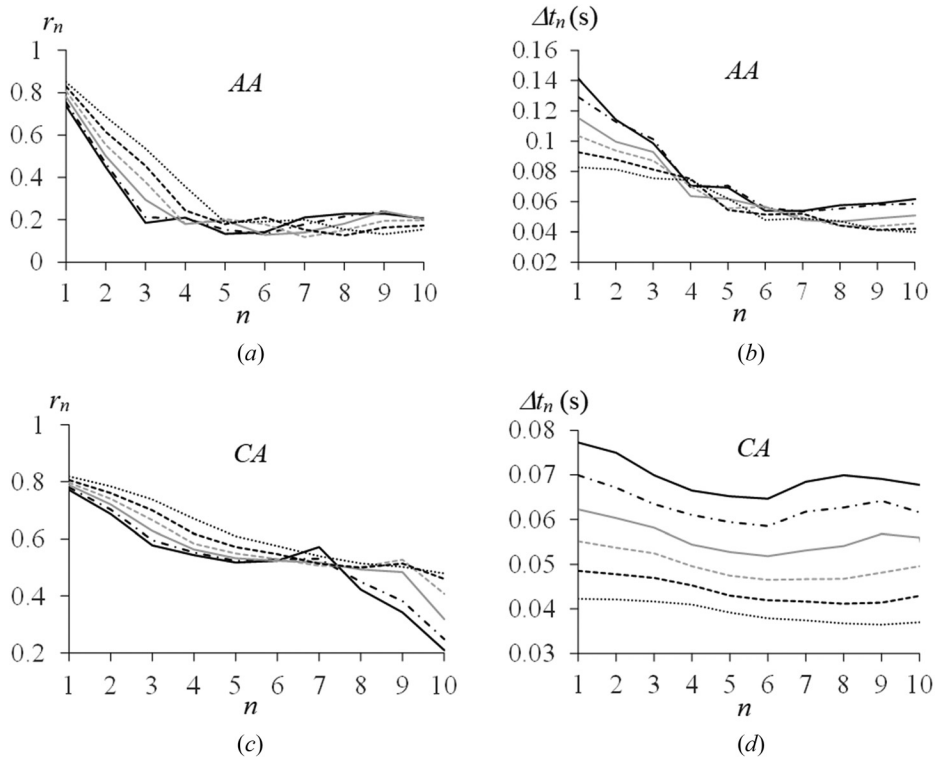

Fig. 8 Wave reflection varies with harmonics at different ages: (*a*) reflection magnitude (*b*) return time at the AA, and (*c*) reflection magnitude (*d*) return time at the CA (25 yr: black solid, 35 yr: black dashdotted, 45 yr: gray solid, 55 yr: gray dashed, 65 yr: black dashed, 75 yr: black dotted)

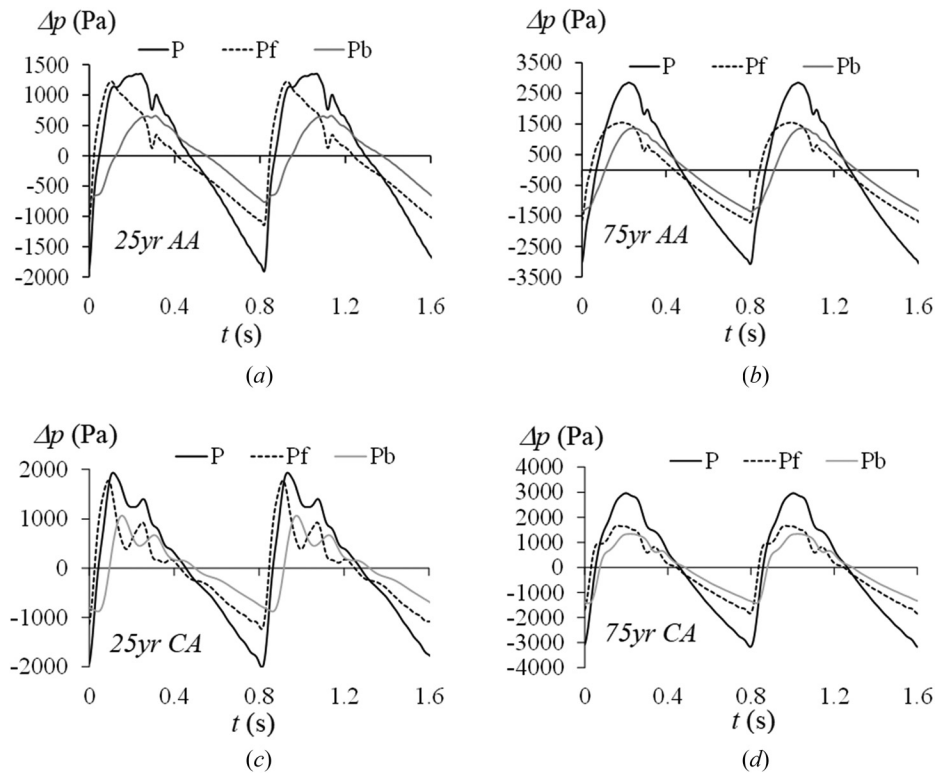

Fig. 9 Pulsatile pressure waveform and its forward waveform and reflected waveform: (*a*) 25 yr, (*b*) 75 yr, at the AA, and (*c*) 25 yr (*d*) 75 yr at the CA (P: pulsatile pressure waveform, Pf: forward pressure waveform, Pb: reflected pressure waveform)

8(*d*), reflection magnitude at the CA goes down very slowly with higher *n*-levels, as compared with its counterpart at the AA. Similar to the AA, the return time for the 1st harmonic is the longest and drops noticeably with aging at the CA. The return time does not decrease much with higher harmonics but decreases with aging for all the harmonics at the CA. The difference in how reflection magnitude and return time vary with harmonics between the AA and the CA might explain why harmonics and waveform of blood velocity show great difference between the two arteries in Fig. 5. Due to harmonics-dependent wave reflection, the forward and the reflected waveforms at the two arteries are quite different, as shown in Fig. 9. Due to significant harmonics-dependence of return time, the foot of reflected waveform at the AA is difficult to identify. In contrast, the foot of reflected waveform at the CA is relatively clear, due to a small variation of return time with harmonics.

3.3 Input Power at the Aorta and Driving Force on the Left Ventricle. To calculate the input power at the AA and the driving force on the LV, the input impedance defined in the vibrating-string model in Eq. (13) is needed. Figure 10 shows how this input impedance at the AA and the CA varies with harmonics at different ages. Note that this input impedance is the reciprocal of the measured input impedance in Fig. 7. As shown in Fig. 11(*a*), based on the vibrating-string model, the input power for the 1st and 2nd harmonics are similar and are dominant at all ages. The input power for the two harmonics become more dominant with aging. Although the input power for the rest harmonics are smaller than that for the 1st and 2nd harmonics, but is non-negligible. In contrast, as shown in Fig. 11(*b*), based on the definition of input power in clinical studies, the input power drops greatly from the 1st harmonic to the 3rd harmonic, with the 1st harmonic being dominant. The input power for the 1st harmonic increases noticeably with aging. The contribution of the 4th *to* 10th harmonics to the input power is negligible at all ages.

As shown in Fig. 12, the driving force amplitude decreases with aging, and no noticeable change in driving force waveform with aging is observed. Note that the values for the LV parameters are kept the same at all ages. The driving force waveform is similar to ECG waveform to some extent [32]. Figure 13 compares the waveforms of pulsatile pressure, blood velocity, and WSS at the AA with the driving force waveform on the LV. While the blood velocity peak is ahead of the pulsatile pressure peak, the WSS peak is ahead of the blood velocity peak. It is interesting to note that the driving force peak is ahead of the blood velocity peak, which is consistent with the clinical finding that an ECG signal is ahead of blood velocity. As such, the driving force might be indicative of an ECG signal. Due to a lack of ECG data in the database, the LV parameters were not adjusted for different ages and no comparison could not be made between the driving force waveform and the ECG waveform.

3.4 Effect of Aging on Harmonics and Waveform of Pulsatile Parameters and 1st Harmonic of Pulsatile Pressure. As shown in Table 1, both arterial stiffness (or PWV) and radius increase with aging at the AA and the CA. Based on Eqs. (7) and (12), both tension and characteristic impedance vary with harmonics, due to fluid-loading. For simplicity, the values for tension T and characteristic impedance Z_c are calculated with exclusion of $1\text{-}F_{10}$, and are included in the table. Tension and characteristic impedance increase with aging at the two arteries. Although PWV is similar at the two arteries, tension and characteristic impedance at the CA are much smaller than their counterparts at the AA, due to the CA being much smaller than the AA. Based on the vibrating-string theory [30,31], characteristic impedance affects harmonics of pulsatile pressure. By comparing characteristic impedance in the table with harmonics of pulsatile pressure in Fig. 4, it might be concluded that high characteristic impedance corresponds to lower harmonics of pulsatile pressure being more dominant relative to higher harmonics. While pulsatile

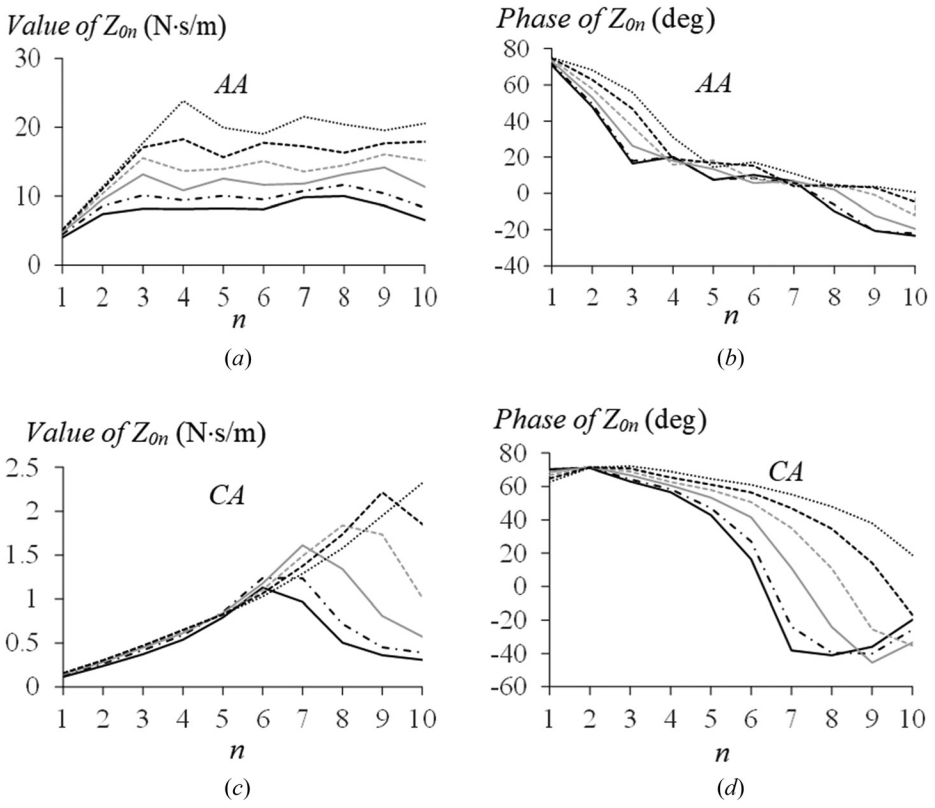

Fig. 10 The input impedance Z_{0n} defined as $F(t)/(\partial\eta/\partial t)$ in the vibrating-string model: (*a*) value (*b*) phase at the AA, and (*c*) value (*d*) phase at the CA (25 yr: black solid, 35 yr: black dashdotted, 45 yr: gray solid, 55 yr: gray dashed, 65 yr: black dashed, 75 yr: black dotted)

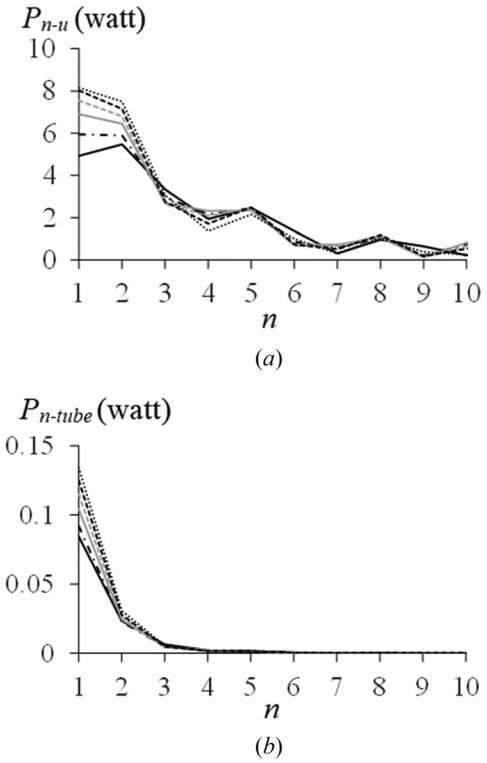

Fig. 11 Input power at the AA varies with harmonics: (*a*) Eq. (17*b*) defined in the vibrating-string model (*b*) Eq. (18) defined in clinical studies (25 yr: black solid, 35 yr: black dashdotted, 45 yr: gray solid, 55 yr: gray dashed, 65 yr: black dashed, 75 yr: black dotted).

pressure amplitude $\Delta p_{\max}$ increases with aging, radial wall displacement amplitude $\eta_{\max}$, blood velocity amplitude $u_{\max}$, and WSS amplitude $\tau_{w\max}$ all decrease with aging at both arteries. The opposite changes between $\Delta p_{\max}$ and the other three pulsatile parameter amplitudes with aging are consistent with the related findings in the literature [3,12].

The difference ($u_{\max}-u_{\min}$) between maximum and minimum of blood velocity and the difference ($\tau_{w\max}-\tau_{w\min}$) between maximum and minimum of WSS are utilized to quantify their respective pulsatility. Meanwhile, time-averaged WSS (TAWSS) over one pulse cycle T for quantifying WSS pulsatility in the literature is defined as [13]

$$\text{TAWSS} = \frac{1}{T}\int_0^T |\tau_w(t)|dt \tag{25}$$

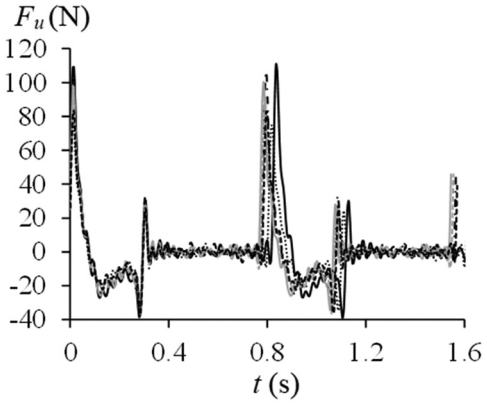

Fig. 12 Driving force waveform at different ages (25 yr: black solid, 35 yr: black dashdotted, 45 yr: gray solid, 55 yr: gray dashed, 65 yr: black dashed, 75 yr: black dotted)

As shown in the table, these three waveform-based indices at the two arteries decrease with aging, consistent with the effect of aging on blood velocity and WSS waveforms in Fig. 3. Reduced pulsatility of blood velocity and WSS is accompanied with lower harmonics of pulsatile pressure being more dominant. Since characteristic impedance affects harmonics of pulsatile pressure, it also affects harmonics of WSS based on Eq. (1*d*). Figure 14 plots two indices for WSS pulsatility versus characteristic impedance. At both arteries, the two indices decrease with characteristic impedance, but their variations with characteristic impedance are different, indicating that harmonics of WSS is manifested differently by the two indices.

Reflection magnitude $r_{\text{whole}} = \Delta p_{f\max}/\Delta p_{b\max}$ of the whole pulsatile pressure waveform in clinical studies is defined as the ratio of the reflected pressure amplitude $\Delta p_{b\max}$ to the forward pressure amplitude $\Delta p_{f\max}$. As shown in Table 1, while r_{whole} increases with aging, $\Delta p_{f\max}$ also increases with aging, indicating that increased $\Delta p_{\max}$ with aging does not solely arise from increased wave reflection [12]. Due to harmonics-dependence of return time, return time and augmentation index (AI) of the whole pulsatile pressure waveform [1] are not calculated.

Given harmonics-dependence of reflection magnitude and return time and dominance of the 1st harmonic in pulsatile pressure, reflection magnitude r_1 and return time Δt_1 of the 1st harmonic of pulsatile pressure are chosen as indices for arterial stiffness and radius (or wave reflection). At both arteries, r_1 increases with aging and Δt_1 decreases with aging. Note that r_1 is always larger than r_{whole}, due to that r_1 is the largest among all the harmonics, and the difference between r_1 and r_{whole}, becomes smaller with aging, because the 1st harmonic becomes more dominant with aging, as shown in Fig. 4. Instead of PWV, it is characteristic impedance at an artery that plays a role in determining wave reflection at it. Figure 15 plots r_{whole}, r_1, and Δt_1 versus characteristic impedance. At both

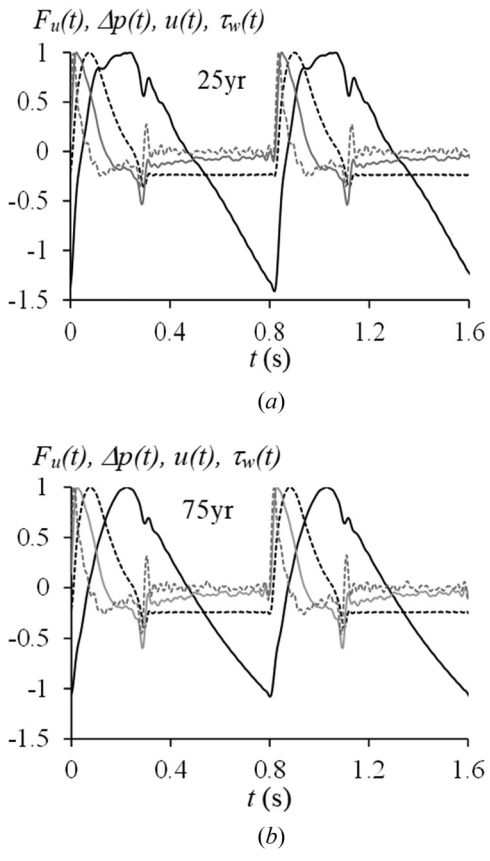

Fig. 13 Normalized waveforms of pulsatile pressure, blood velocity, and WSS at the AA and driving force on the LV: (*a*) 25 yr (*b*) 75 yr ($F_u(t)$: gray dashed, $\Delta p(t)$: black solid, $u(t)$: black dashed, $\tau_w(t)$: gray solid)

arteries, while r_1 and Δt_1 vary smoothly with characteristic impedance, r_{whole} increases nonsmoothly with characteristic impedance.

4 Discussion

In this study, harmonics of pulsatile pressure at different ages and its effect on other pulsatile parameters and waveform-based clinical indices are calculated. As shown in Sec. 3, on the one hand, harmonics of a pulsatile parameter plays a role in determining its waveform and consequently waveform-based clinical indices. On the other hand, wave transmission and wave reflection also affect waveform of a pulsatile parameter, and are both harmonics dependent. The arterial tree is not infinitely long, with one end connected to the LV starting pulsatile waves and the other end at termination. Wave reflection at any position along the arterial tree is affected by termination. Yet, the majority of the studies on pulsatile pressure waveform have focused on correlating arterial stiffness and radius to wave transmission and wave reflection for pulsatile pressure waveform, with no consideration of harmonics-dependence of wave transmission, wave reflection, and the finite length of the arterial tree. As such, in the context of the whole system: the LV, the arterial tree, and termination, we explore possible affecting factors of wave transmission, wave reflection, and harmonics of pulsatile pressure, based on the analyzed results. Afterwards, we clarify inconsistency of some definitions in clinical studies with their physical implications and physical implications of waveform-based clinical indices. Based on the difference in harmonics of pulsatile pressure at different ages and between the two arteries, physiological implications and potential clinical applications of the analyzed results are discussed.

Table 1 Effect of aging on arterial properties and geometries, pulsatile parameter amplitudes, waveform-based clinical indices, and indices of the 1st harmonic (*a*) at the AA (*b*) at the CA

(a)

Age (yr)		25	35	45	55	65	75
HR (bpm)		72.82	76.73	77.72	77.32	76.53	74.44
Arterial properties and geometries	a (mm)	18.36	18.94	19.50	20.06	20.64	21.23
	Eh	1306	1629	2148	2770	3539	4524
	T (N)	37.63	48.44	65.78	87.26	114.65	150.79
	Z_c (N·s/m)	6.52	7.63	9.15	10.84	12.78	15.08
	PWV (m/s)	5.78	6.35	7.19	8.05	8.97	10.00
Pulsatile parameter amplitudes	$\Delta p_{\max}$ (Pa)	3275	3485	4032	4606	5190	5881
	$\eta_{\max}$ (mm)	0.85	0.77	0.71	0.67	0.62	0.59
	$u_{\max}$ (m/s)	0.376	0.340	0.309	0.280	0.254	0.229
	$\tau_{w\max}$ (Pa)	2.63	2.37	2.14	1.94	1.73	1.58
Waveform-based clinical indices	$u_{\max}$ (m/s)	0.376	0.340	0.309	0.280	0.254	0.229
	$u_{\min}$ (m/s)	−0.044	−0.041	−0.038	−0.036	−0.034	−0.032
	$u_{\max}-u_{\min}$ (m/s)	0.420	0.381	0.347	0.316	0.288	0.261
	$\tau_{w\max}$ (Pa)	2.63	2.37	2.14	1.94	1.73	1.58
	$\tau_{w\min}$ (Pa)	−1.16	−1.05	−0.99	−0.90	−0.84	−0.75
	$\tau_{w\max}-\tau_{w\min}$ (Pa)	3.80	3.43	3.13	2.84	2.56	2.33
	$TAWSS$ (Pa)	0.49	0.46	0.42	0.38	0.34	0.30
	$\Delta p_{f\max}$ (Pa)	2672	2677	2800	2933	3148	3432
	$\Delta p_{b\max}$ (Pa)	1531	1638	1898	2154	2431	2763
	r_{whole}	0.57	0.61	0.68	0.73	0.77	0.81
Indices of the 1st harmonic	r_1	0.74	0.76	0.78	0.81	0.83	0.85
	Δt_1 (s)	0.1413	0.1292	0.1154	0.1035	0.0927	0.0827

(b)

Age (yr)		25	35	45	55	65	75
HR (bpm)		72.82	76.73	77.72	77.32	76.53	74.44
Arterial property and geometry	a (mm)	4.37	4.52	4.66	4.80	4.94	5.08
	Eh	330	412	543	701	896	1147
	T (N)	2.26	2.92	3.97	5.27	6.94	9.15
	Z_c (N·s/m)	0.38	0.45	0.54	0.64	0.75	0.89
	PWV (m/s)	5.95	6.54	7.40	8.28	9.23	10.29
Pulsatile parameter amplitude	$\Delta p_{\max}$ (Pa)	3948	3989	4283	4877	5475	6136
	$\eta_{\max}$ (mm)	0.23	0.20	0.17	0.16	0.15	0.14
	$u_{\max}$ (m/s)	0.427	0.382	0.336	0.293	0.252	0.215
	$\tau_{w\max}$ (Pa)	2.90	2.64	2.38	2.15	1.91	1.68
Waveform-based indices	$u_{\max}$ (m/s)	0.427	0.382	0.336	0.293	0.252	0.215
	$u_{\min}$ (m/s)	−0.011	−0.013	−0.008	−0.001	−0.001	0.002
	$u_{\max}-u_{\min}$ (m/s)	0.438	0.394	0.344	0.294	0.254	0.213
	$\tau_{w\max}$ (Pa)	2.90	2.64	2.38	2.15	1.91	1.68
	$\tau_{w\min}$ (Pa)	−1.74	−1.45	−1.10	−0.75	−0.67	−0.60
	$\tau_{w\max}-\tau_{w\min}$ (Pa)	4.64	4.09	3.48	2.90	2.59	2.28
	TAWSS (Pa)	0.54	0.48	0.40	0.33	0.27	0.22
	Δp_{fmax} (Pa)	3007	2941	2965	2939	3188	3509
	Δp_{bmax} (Pa)	1947	1939	1985	2204	2463	2768
	r_{whole}	0.65	0.66	0.67	0.75	0.77	0.79
Indices of the 1st harmonic	r_1	0.77	0.78	0.79	0.80	0.81	0.82
	Δt_1 (s)	0.0773	0.0699	0.0623	0.0552	0.0485	0.0422

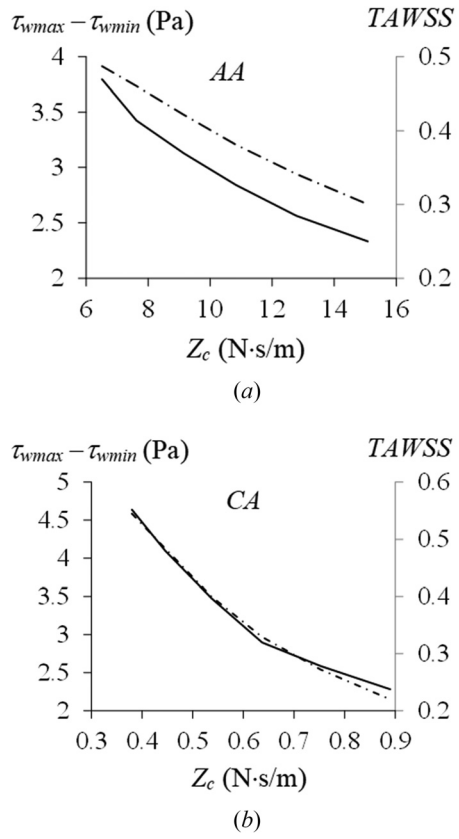

Fig. 14 Two indices for WSS pusaltility: $\tau_{wmax}-\tau_{wmin}$ and *TAWSS*, versus characteristic impedance: (*a*) at the AA (*b*) at the CA ($\tau_{wmax}-\tau_{wmin}$: solid, TAWSS: dashdotted)

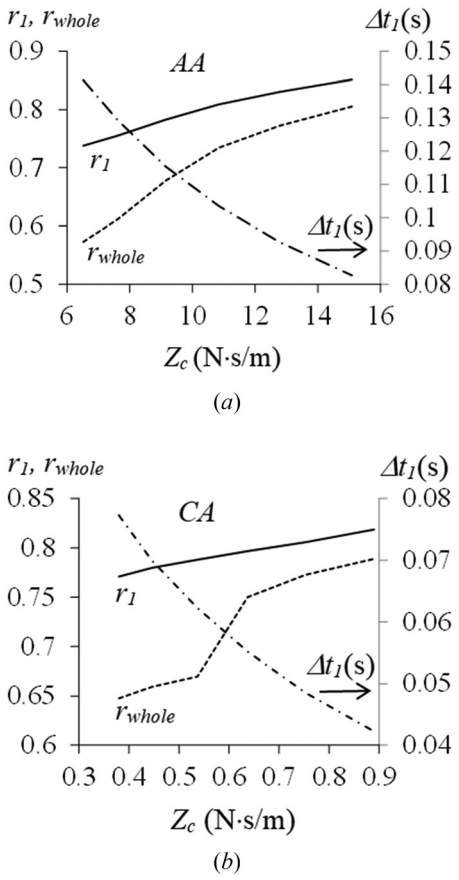

Fig. 15 Reflection magnitude r_1 and return time Δt_1 of the 1st harmonics and reflection magnitude r_{whole} of the whole waveform versus characteristic impedance: (*a*) at the AA (*b*) at the CA (r_1: solid, r_{whole}: dashed, Δt_1: dashdotted)

4.1 Affecting Factors of Wave Transmission, Wave Reflection, and Harmonics of Pulsatile Pressure. Wave transmission is quantified by wave number and transmission loss, as shown in Eq. (9). It is solely determined by arterial stiffness (i.e., *PWV*) and radius (accounting for 1-F_{10}). Due to harmonics-dependence of fluid-loading F_{10}, each harmonic transmits at its own velocity with its own transmission loss. Thus, the forward waveform varies along the arterial tree. As shown in Fig. 16, the arterial tree involves dramatic nonuniformity (i.e., tapered geometry, varying elasticity, and branching sites). Arterial nonuniformity complicates harmonics-dependence of wave transmission and wave reflection in the arterial tree. Wave velocity in Eq. (4) is local wave velocity at a position in an arterial segment for calculating local wave transmission and local wave reflection in the segment.

Wave reflection occurs whenever there is an impedance mismatch [30]. As shown in Fig. 16, the *n*th load impedance Z_{Ln} at position x is the sum of the *n*th characteristic impedance Z_{cn2} for the rest arterial section: $x \in (x, L_T)$ and the *n*th termination impedance Z_{Tn}. The *n*th reflection coefficient at position x is:

$$R_n = \frac{1 - Z_{Ln}/Z_{cn1}}{1 + Z_{Ln}/Z_{cn1}} \text{ with } Z_{Ln} = Z_{cn2} + Z_{Tn} \tag{26}$$

where Z_{cn1} is the *n*th characteristic impedance at position x. Harmonics-dependence of termination impedance is caused by the variation of characteristic impedance along the arterial tree, which arises from arterial nonuniformity [18,19,30]. Meanwhile, harmonics-dependence of Z_{cn2} is also affected by arterial nonuniformity. As such, arterial nonuniformity renders harmonics-dependence of Z_{Ln} at any position theoretically unpredictable, as exemplified by load impedance at the AA and the CA. As expressed in Eq. (26), it is the ratio of load impedance to characteristic impedance that determines wave reflection at an artery. This may explain why wave reflection at an artery is more than its stiffness and radius [3]. As shown in Fig. 17, the 1st load impedance at the two arteries increases nonlinearly with characteristic impedance, but the ratio of the 1st load impedance to characteristic impedance decreases with high characteristic impedance, leading to increased 1st reflection magnitude.

As shown in Fig. 2(*a*), when the driving force on the LV excites pulsatile waves, the arterial tree and termination interfere with the LV response. As such, harmonics of pulsatile pressure at any position along the arterial tree is determined by the LV [7], characteristic impedance of the arterial tree, and termination impedance. As shown in Sec. 3, The change in harmonics of pulsatile pressure with aging is accompanied by the age-related change in characteristic impedance of the arterial tree and the input impedance at the AA (indicative of termination impedance). Due to a lack of ECG data, how the LV affects harmonics of pulsatile pressure cannot be examined here. Table 2 summarizes the affecting

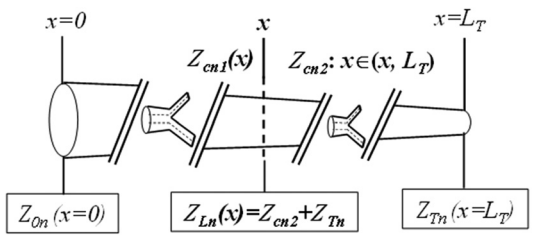

Fig. 16 Arterial nonuniformity complicates wave transmission and wave reflection at any position along the arterial tree

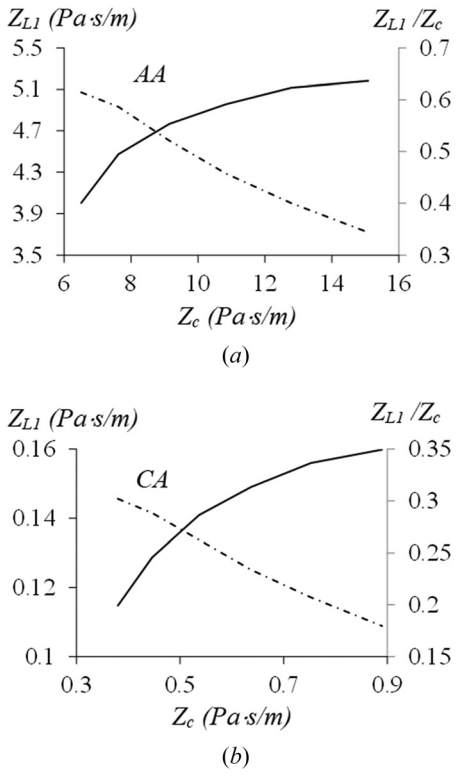

Fig. 17 The 1st load impedance Z_{L1} and ratio of Z_{L1}/Z_c versus characteristic impedance Z_c (excluding *1-F*$_{10}$): (*a*) at the AA (*b*) at the CA (Z_{L1}: solid, Z_{L1}/Z_c: dashedotted)

factors of wave transmission, wave reflection, and harmonics of pulsatile pressure.

4.2 Inconsistency of Input Impedance and Input Power in Clinical Studies With Their Physical Implications. Input impedance $Z_{0n\text{-meas}}$ at the AA in clinical studies is defined as the ratio of pulsatile pressure versus blood velocity, $\Delta p(t)/u(t)$. In the vibrating-string model, this input impedance Z_{0n} is defined as the ratio of driving force versus radial wall velocity, $F(t)/(\partial\eta/\partial t)$. According to Eq. (20), Z_{0n} is the reciprocal of $Z_{0n\text{-meas}}$. The definition of $Z_{0n\text{-meas}}$ is inconsistent with its physical implication as a measure of resistance to flow upon effort [27,28], because $Z_{0n\text{-meas}}$ at the AA in Figs. 7(*a*) and 7(*b*) indicates that (1) the highest $Z_{0n\text{-meas}}$ for the 1st harmonic should cause the smallest amplitude of pulsatile pressure, but the 1st harmonic of pulsatile pressure in Fig. 4(*a*) is the largest; and (2) the negative phase of $Z_{0n\text{-meas}}$ indicates that blood velocity causes pulsatile pressure. In contrast, as shown in Fig. 10, the definition of Z_{0n} is consistent with its physical implication: the lowest Z_{0n} for the 1st harmonics translates to the largest amplitude of radial wall displacement (i.e., pulsatile pressure, see Eq. (3)) and positive phase of Z_{0n} indicates that driving force causes radial wall displacement. Most importantly, the definition of input impedance in the vibrating-string model allows examining the LV-artery interaction to relate ECG signals to pulsatile pressure in the arterial tree and explore the influence of the LV function on harmonics of pulsatile pressure. Yet, due to its inconsistency with its physical implications in the 1D wave propagation context, input impedance in clinical studies is unsuitable for studying the LV-artery interaction [19].

Similarly, the definition of the input power in Eq. (18) in clinic studies indicates that only the first three harmonics are relevant to energy transmission along the arterial tree, as shown in Fig. 11(*b*). Yet, higher harmonics have been found to be important to CV physiology, such as higher harmonics of WSS contributing to a larger WSS amplitude [8] and EC sensitivity to harmonics of WSS [26,27]. In contrast, as shown in Fig. 11(*a*), the definition of the input power in Eq. (17*b*) shows that contribution of higher harmonics to the input power are non-negligible, indicating that they also play a role in CV physiology. Furthermore, Eq. (17*b*) is analogous to timbre (the mix of different harmonics) generated by a musical instrument. All the harmonics in a musical instrument make non-negligible contributions to timbre for enriching the sound [31].

4.3 Waveform-Based Clinical Indices. At the CA, defined as the difference between u_{max} and u_{min} divided by the mean value of $u(t)$, FPI is a measure of blood velocity pulsatility [12]. FFT analysis shifts blood velocity waveform by a unknown constant, and thus its mean value cannot be obtained. However, $u_{max}-u_{min}$ captures blood velocity pulsatility. TAWSS and $\tau_{wmax}-\tau_{wmin}$ captures WSS pulsatility. The cause underlying these indices is harmonics of pulsatile pressure. While harmonics of WSS is dictated by harmonics of pulsatile pressure, it is an important determinant of endothelial function. As such, harmonics of pulsatile pressure can serve as an independent clinical index indicative of endothelial function.

At the AA, waveform-based clinical indices: reflection magnitude, return time, and AI, are all defined based on the whole pulsatile pressure waveform [1,2,4–8,18]. As analyzed in Sec. 3, due to harmonics-dependence of wave transmission and wave reflection, reflection magnitude based on the whole waveform is a composite of the reflection magnitudes and reflection phases for all the harmonics. Since it manifests harmonics of pulsatile pressure, it is more than arterial stiffness and radius [3]. Similarly, as a composite indicator of reflection magnitude and return time for the reflected waveform, AI manifests both wave reflection for all the harmonics and harmonics of pulsatile pressure [19]. Since harmonics in the reflected waveform return to the AA at different times, definition of return time for the reflected waveform is inconsistent with physiological reality. This explains the difficulty in identifying the foot of the reflected waveform [1,2]. As compared with reflection magnitude and AI for the whole waveform reflection magnitude and return time for the 1st harmonic serves better as clinical indices for arterial stiffness and radius.

As compared with arterial stiffness, these waveform-based clinical indices at the CA and the AA have been found to carry their independent values [1–15]. As analyzed here, their independent clinical values stem from harmonics of pulsatile pressure, which is determined by the LV, the arterial tree, and termination. Yet, these waveform-based clinical indices manifest harmonics of a pulsatile parameter to a limited extent. In particular, return time and AI is against physiological reality. In recent years, changes in different harmonics of pulsatile pressure at the RA have been correlated with different conditions [20–25]. As such, harmonics of pulsatile pressure need to serve as an independent clinical index indicative of the LV function.

4.4 Physiological Implications and Potential Clinical Applications. Harmonics of pulsatile pressure varies with aging, and dictates harmonics of blood velocity and WSS. As compared with at old age, lower harmonics of pulsatile pressure and input power are found to be less dominant relative to higher harmonics at young age. In contrast, as compared with at old age, lower harmonics of WSS is more dominant relative to higher harmonics at young age. This might imply that low wave reflection contributes more to increase the amplitudes of lower harmonics of WSS at young age, despite their low amplitudes in the forward waves. In contrast, high wave reflection might contribute less to increase the amplitudes of lower harmonics of WSS at old age, despite their increased amplitudes in the forward waves. In other words, wave reflection affects the amplitudes of lower harmonics of WSS to a greater extent, as compared with their amplitudes in the forward waves. Since lower harmonics of pulsatile pressure being more dominant translates to high WSS amplitude and WSS pulsatility, it carries physiological significance to endothelial function.

Harmonics of pulsatile pressure varies between the AA and the CA. As compared with lower harmonics, higher harmonics of

Table 2 Affecting factors of wave transmission, wave reflection, and harmonics of pulsatile pressure

Component	Parameters	Wave transmission: k_n & γ_n	Wave reflection: R_n	Harmonics of $\Delta p\ (x, t)$: $\sum_n \Delta p_n \cos(n\omega t + \alpha_n)$
LV Arterial tree Termination	M, K, D c_n, Z_{cn} Z_{Tn}	k_n & $\gamma_n \propto n\omega/c_n$	$R_n = \dfrac{1 - Z_{Ln}/Z_{cn1}}{1 + Z_{Ln}/Z_{cn1}}$ $(Z_{Ln} = Z_{cn2} + Z_{Tn})$	$\sum_n \Delta p_n \cos(n\omega t + \alpha_n) \propto$ function $(M, K, D, Z_{cn}, Z_{Tn})$

pulsatile pressure are more noticeable at the CA than at the AA. Due to the difference in wave reflection between the two arteries, although the 1st and 2nd harmonics of WSS at the AA are much higher than their counterparts at the AA, the 3rd ∼ 6th harmonics of WSS at the CA are much higher than their counterparts at the AA. This explains why WSS waveform at the CA is much more oscillatory than that at the AA, as shown in Fig. 3. Although *TAWSS* and $\tau_{wmax} - \tau_{wmin}$ manifest the change in WSS oscillatory level at different ages at each artery, they are not comparable between the two arteries, as shown in Table 1. This might be caused by the difference in WSS waveform between the two arteries. Given that harmonics of pulsatile pressure varies with CV conditions, it is expected that WSS waveform varies with CV conditions and then these two pulsatility indices are insufficient for comparing WSS oscillatory levels between CV conditions.

From the AA to the CA, pulsatile pressure travels from larger arteries to small arteries and passes through branching sites in between. It is believed that branching sites function as boundaries for an arterial segment [33], causing mode-coupling (or energy transfer) between different *n*-levels of pulsatile pressure and leading to difference in harmonics of pulsatile pressure between the two arteries. Consequently, harmonics of WSS is also modified by branching sites, leading to high oscillatory level in WSS waveform at the CA. Given its small size, high oscillatory level of WSS waveform at the CA might improve its physiological function for delivering nutrients and oxygen to the body. This might explain why pulmonary vasculature forms a rapidly branching arterial network [34]. Small size of arteries in it might demand a much higher oscillatory level of WSS waveform to perfuse the lungs and oxygenate blood.

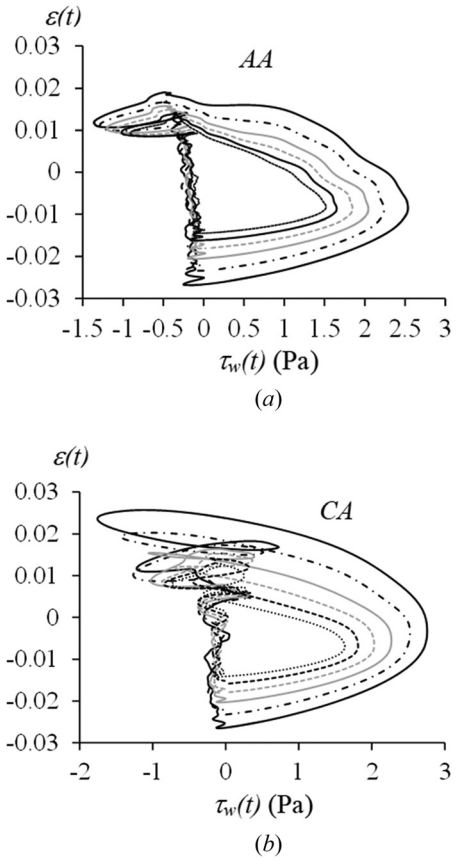

Fig. 18 WSS-CS loop (or $\tau_w(t) \sim \varepsilon(t)$ loop) at different ages: (*a*) at the AA (*b*) at the CA (25 yr: black solid, 35 yr: black dashdotted, 45 yr: gray solid, 55 yr: gray dashed, 65 yr: black dashed, 75 yr: black dotted)

Given synergistic effects of WSS and CS ($\varepsilon = \eta(t)/a$) in the arterial wall on endothelial function [28], WSS-CS loops at different ages are plotted in Fig. 18. Although the sizes of the WSS-CS loops shrink with aging, their shapes remain the same at each artery. Given that these loops correspond to healthy subjects at different ages, it might be concluded that the shape of a WSS-CS loop is more indicative of endothelial function, instead of its size.

Wang et al. [35] examined harmonics of pulsatile pressure at the radial artery (RA) and found that aging increases the 1st harmonic, decreases the *3rd* and *4th* harmonics, and has no effect on the 2nd harmonic. In contrast, the 1st and *2nd* harmonics at the AA and the CA both reveal a noticeable increase with aging, as shown in Fig. 4. Meanwhile, different conditions, such as coronary artery disease, diabetes, and Alzheimer's disease were found to affect different *n*-levels of pulsatile pressure at the RA [20–25]. Based on the analyzed results here, it is believed that any changes in the arterial tree, such as vasoconstriction, occlusion and vasodilation, and any events, such as hypoxia, will affect characteristic impedance and termination impedance in the arterial tree and accordingly the LV function, due to the LV-artery interaction. Then, harmonics of pulsatile pressure at all the arteries is expected to change and it can only be obtained from measurement under these conditions. Thus, harmonics of pulsatile pressure at an artery can serve as an independent clinical index indicative of the LV function. To separate the influence of the LV on harmonics of pulsatile pressure from the influence of the arterial tree and termination, ECG signals need to be related to pulsatile parameters at an artery for quantifying the LV.

Although pulsatile parameters at the AA are more relevant to the LV function [1], their measurement poses significant challenges. In contrast, pulsatile parameters at the CA are commonly measured in clinical studies and also reveal difference with aging. As such, instead of the AA, it might be more practical to characterize pulsatile parameters at the CA under different conditions for inferring the LV function. Taken together, harmonics of pulsatile pressure at the two arteries can serve as a clinical index indicative of the LV function and endothelial function, and reflection magnitude and return time of the 1st harmonics at the two arteries can serve as two clinical indices indicative of arterial stiffness and radius. WSS-CS loop might serve as a clinical index for diagnosing the onset of atherosclerosis, given that endothelial dysfunction occurs prior to arterial stiffening. Easy access to the CA will allow routine measurement of these clinical indices. In the future, ECG data needs to be related to pulsatile pressure and blood flow at the two arteries for quantifying the LV and its influence on harmonics of pulsatile pressure.

5 Conclusion

By applying a vibrating-string model of the arterial tree to the related data in a database, this study examines harmonics of pulsatile

pressure at different ages and its effect on other pulsatile parameters and waveform-based clinic indices. Harmonics of pulsatile pressure, blood velocity, and WSS varies with aging and between the AA and the CA. As compared with lower harmonics, higher harmonics of pulsatile pressure, blood velocity, and WSS are more noticeable at the CA than at the AA. With aging, lower harmonics of pulsatile pressure and input power increase, but lower harmonics of blood velocity and WSS decrease. It is found that high characteristic impedance (i.e., arterial stiffness and radius) at the two arteries is associated with lower harmonics of pulsatile pressure being more dominant relative to its higher harmonics and reduced WSS oscillatory level.

The entangled relations of wave transmission, wave reflection, and harmonics of pulsatile pressure to the whole CV system: the LV, arterial tree, and termination, are clarified. While wave transmission is solely determined by arterial stiffness and radius, wave reflection is determined by arterial stiffness and radius and termination impedance. Arterial nonuniformity causes unpredictable harmonics-dependence of wave reflection. Consequently, reflection magnitude and return time vary between harmonics. Reflection magnitude based on the whole waveform is unsuitable for indicating arterial stiffness and radius, and definitions of return time and AI based on the whole waveform are inconsistent with physiological reality. Harmonics of pulsatile pressure is a combination of the LV, the arterial tree, and termination, and carries its independent clinical values, as compared with arterial stiffness and radius. As such, it is suggested that harmonics of pulsatile pressure serves as an independent clinical index indicative of the LV function and endothelial function, and reflection magnitude and return time for the 1st harmonics of pulsatile pressure serve as clinical indices indicative of arterial stiffness and radius.

References

[1] Westerhof, B. E., and Westerhof, N., 2018, "Uniform Tube Models With Single Reflection Site Do Not Explain Aortic Wave Travel and Pressure Wave Shape," Physiol. Meas., **39**(12), p. 124006.

[2] Westerhof, B. E., and Westerhof, N., 2012, "Magnitude and Return Time of the Reflected Wave: The Effects of Large Artery Stiffness and Aortic Geometry," J. Hypertens., **30**(5), pp. 932–939.

[3] Mitchell, G. F., van Buchem, M. A., Sigurdsson, S., Gotal, J. D., Jonsdottir, M. K., Kjartansson, Ó., Garcia, M., et al., 2011, "Arterial Stiffness, Pressure and Flow Pulsatility and Brain Structure and Function: The Age, Gene/Environment Susceptibility–Reykjavik Study," Brain, **134**(11), pp. 3398–3407.

[4] Torjesen, A. A., Wang, N., Larson, M. G., Hamburg, N. M., Vita, J. A., Levy, D., Benjamin, E. J., Vasan, R. S., and Mitchell, G. F., 2014, "Forward and Backward Wave Morphology and Central Pressure Augmentation in Men and Women in the Framingham Heart Study," Hypertension, **64**(2), pp. 259–265.

[5] Kaya, M., Balasubramanian, V., and Li, J. K., 2022, "Inadequacy of Augmentation Index for Monitoring Arterial Stiffness: Comparison With Arterial Compliance and Other Hemodynamic Variables," Cardiovasc. Eng. Technol., **13**(4), pp. 590–602.

[6] Hughes, A. D., Park, C., Davies, J., Francis, D., McG Thom, S. A., Mayet, J., and Parker, K. H., 2013, "Limitations of Augmentation Index in the Assessment of Wave Reflection in Normotensive Healthy Individuals," PLoS One, **8**(3), p. e59371.

[7] Heusinkveld, M. H. G., Delhaas, T., Lumens, J., Huberts, W., Spronck, B., Hughes, A. D., and Reesink, K. D., 2019, "Augmentation Index is Not a Proxy for Wave Reflection Magnitude: Mechanistic Analysis Using a Computational Model," J. Appl. Physiol., **127**(2), pp. 491–500.

[8] Du, S., Liu, W., Yao, Y., Sun, G., He, Y., Alastruey, J., Xu, L., Yao, Y., and Qian, W., 2022, "Reconstruction of the Aortic Pressure Waveform Using a Two-Level Adaptive Transfer Function Strategy," Measurement, **204**, p. 112111.

[9] Hitomi, Y., Masaki, N., Ishinoda, Y., Kagami, K., Yasuda, R., Toya, T., Namba, T., Nagatomo, Y., Takase, B., and Adachi, T., 2022, "Effectiveness of Pulsatility Index of Carotid Doppler Ultrasonography to Predict Cardiovascular Events," J. Med. Ultrason., **49**(1), pp. 95–103.

[10] Chuang, S. Y., Cheng, H. M., Bai, C. H., Yeh, W. T., Chen, J. R., and Pan, W. H., 2016, "Blood Pressure, Carotid Flow Pulsatility, and the Risk of Stroke: A Community-Based Study," Stroke, **47**(9), pp. 2262–2268.

[11] Ozari, H. O., Oktenli, C., Celik, S., Tangi, F., Ipcioglu, O., Terekeci, H. M., Top, C., Uzun, M., Sanisoglu, Y. S., and Nalbant, S., 2012, "Are Increased Carotid Artery Pulsatility and Resistance Indexes Early Signs of Vascular Abnormalities in Young Obese Males?," J. Clin. Ultrasound, **40**(6), pp. 335–340.

[12] Heffernan, K. S., Spartano, N. L., Augustine, J. A., Lefferts, W. K., Hughes, W. E., Mitchell, G. F., Jorgensen, R. S., and Gump, B. B., 2015, "Carotid Artery Stiffness and Hemodynamic Pulsatility During Cognitive Engagement in Healthy Adults: A Pilot Investigation," Am. J. Hypertens., **28**(5), pp. 615–622.

[13] Peiffer, V., Sherwin, S. J., and Weinberg, P. D., 2013, "Does Low and Oscillatory Wall Shear Stress Correlate Spatially With Early Atherosclerosis? A Systematic Review," Cardiovasc. Res., **99**(2), pp. 242–250.

[14] Avrahami, I., Kersh, D., and Liberzon, A., 2016, "Pulsatility Index as a Diagnostic Parameter of Reciprocating Wall Shear Stress Parameters in Physiological Pulsating Waveforms," PLoS One, **11**(11), p. e0166426.

[15] Liu, H. B., Yuan, W. X., Qin, K. R., and Hou, J., 2015, "Acute Effect of Cycling Intervention on Carotid Arterial Hemodynamics: Basketball Athletes Versus Sedentary Controls," Biomed. Eng. Online, **14**(S1), p. S17.

[16] Qureshi, M. U., Colebank, M. J., Schreier, D. A., Tabima, D. M., Haider, M. A., Chesler, N. C., and Olufsen, M. S., 2018, "Characteristic Impedance: Frequency or Time Domain Approach?," Physiol. Meas., **39**(1), p. 014004.

[17] Willemet, M., and Alastruey, J., 2015, "Arterial Pressure and Flow Wave Analysis Using Time-Domain 1-D Hemodynamics," Ann. Biomed. Eng, **43**(1), pp. 190–206.

[18] Mynard, J. P., Kondiboyina, A., Kowalski, R., Cheung, M. M. H., and Smolich, J. J., 2020, "Measurement, Analysis and Interpretation of Pressure/Flow Waves in Blood Vessels," Front. Physiol., **11**, p. 1085.

[19] Hao, Z., 2023, "A Vibrating-String Model for Closed-Loop Wave Transmission and Reflection Between the Aorta and Periphery," ASME J Med. Diagn., **6**(4), p. 041001.

[20] Chang, C. W., Liao, K. M., Chang, Y. T., Wang, S. H., Chen, Y. C., and Wang, G. C., 2019, "Fourth Harmonic of Radial Pulse Wave Predicts Adverse Cardiac Events in Asymptomatic Patients With Type 2 Diabetes," J. Diabetes Complications, **33**(6), pp. 413–416.

[21] Hsiu, H., Liu, J. C., Yang, C. J., Chen, H. S., Wu, M. S., Hao, W. R., Lee, K. Y., et al., 2022, "Discrimination of Vascular Aging Using the Arterial Pulse Spectrum and Machine-Learning Analysis," Microvasc. Res., **139**, p. 104240.

[22] Chang, C. W., Liao, K. M., Chang, Y. T., Wang, S. H., Chen, Y. C., and Wang, G. C., 2018, "The First Harmonic of Radial Pulse as an Early Predictor of Silent Coronary Artery Disease and Adverse Cardiac Events in Type 2 Diabetic Patients," Cardiol. Res. Pract., **2018**, pp. 1–9.

[23] Huang, Y. C., Chang, Y. H., Cheng, S. M., Lin, S. J., Lin, C. J., and Su, Y. C., 2019, "Applying Pulse Spectrum Analysis to Facilitate the Diagnosis of Coronary Artery Disease," Evidence-Based Complementary Altern. Med., **2019**, pp. 1–10.

[24] Lin, S. K., Hsiu, H., Chen, H. S., and Yang, C. J., 2021, "Classification of Patients With Alzheimer's Disease Using the Arterial Pulse Spectrum and a Multilayer-Perceptron Analysis," Sci. Rep., **11**(1), p. 8882.

[25] Chen, P.-J., Wu, H.-K., Hsu, P.-C., Lo, L.-C., Chang, H.-H., and Worsnop, C., 2020, "Effects of Five Daily Activities on Harmonic Analysis of the Radial Pulse," Evidence-Based Complementary Altern. Med., **2020**, pp. 1–5.

[26] Baeyens, N., Bandyopadhyay, C., Coon, B. G., Yun, S., and Schwartz, M. A., 2016, "Endothelial Fluid Shear Stress Sensing in Vascular Health and Disease," J. Clin. Invest., **126**(3), pp. 821–828.

[27] Feaver, R. E., Gelfand, B. D., and Blackman, B. R., 2013, "Human Haemodynamic Frequency Harmonics Regulate the Inflammatory Phenotype of Vascular Endothelial Cells," Nat. Commun., **4**(1), p. 1525.

[28] Zhao, S., Suciu, A., Ziegler, T., Moore, J. E., Bürki, E., Meister, J.-J., and Brunner, H. R., 1995, "Synergistic Effects of Fluid Shear Stress and Cyclic Circumferential Stretch on Vascular Endothelial Cell Morphology and Cytoskeleton," Arterioscler. Thromb. Vasc. Biol., **15**(10), pp. 1781–1786.

[29] Charlton, P. H., Mariscal, H. J., Vennin, S., Li, Y., Chowienczyk, P., and Alastruey, J., 2019, "Modelling Arterial Pulse Waves in Healthy Ageing: A Database for in Silico Evaluation of Haemodynamics and Pulse Wave Indices," Am. J. Physiol. Heart Circ. Physiol., **317**(5), pp. H1062–H1085.

[30] Kinsler, L. E., Frey, A. R., Coppens, A. B., and Sanders, J. V., 2000, "*Fundamentals of Acoustics*," 4th ed., Wiley Inc., Hoboken, NJ.

[31] Raichel, D. R., 2006, *The Science and Applications of Acoustics*, Springer Science & Business Media, Berlin.

[32] Zhu, Q., Tian, X., Wong, C. W., and Wu, M., 2021, "Learning Your Heart Actions From Pulse: ECG Waveform Reconstruction From PPG," IEEE Internet Things J., **8**(23), pp. 16734–16748.

[33] Tokunaga, T., Mori, K., Kadowaki, H., and Saito, T., 2020, "Study on Natural Vibration Characteristics Based on the Coupled Wave Theory of Spring Supported Elastic Pipes and Fluids," ASME Paper No. V005T05A076.

[34] Chesler, N. C., Roldan, A., Vanderpool, R. R., and Naeije, R., 2009, "How to Measure Pulmonary Vascular and Right Ventricular Function," Annu. Int. Conf. IEEE Eng. Med. Biol. Soc., **2009**, pp. 177–180.

[35] Wang, S. H., Hsu, T. L., Jan, M. Y., Wang, Y. Y. L., and Wang, W. K., 2009, "Age-Related Changes in Specific Harmonic Indices of Pressure Pulse Waveform," 13th International Conference on Biomedical Engineering, Lim, C. T., and Goh, J. C. H. eds., Vol. 23, Springer, Berlin, Heidelberg, pp. 183–185.